

NEUROFLEX: COLUMN-EXACT ANN-SNN CO-EXECUTION ACCELERATOR WITH COST-GUIDED SCHEDULING

Varun Manjunath¹ Pranav Ramesh¹ Gopalakrishnan Srinivasan¹

ABSTRACT

NeuroFlex is a column-level accelerator that co-executes artificial and spiking neural networks to minimize energy–delay product on sparse edge workloads with competitive accuracy. The design extends integer-exact QCFS ANN-SNN conversion from layers to independent columns. It unifies INT8 storage with on-the-fly spike generation using an offline cost model to assign columns to ANN or SNN cores and pack work across processing elements with deterministic runtime. Our cost-guided scheduling algorithm improves throughput by 16–19% over random mapping and lowers EDP by 57–67% versus a strong ANN-only baseline across VGG-16, ResNet-34, GoogLeNet, and BERT models. NeuroFlex also delivers up to $2.5\times$ speedup over LoAS and $2.51\times$ energy reduction over SparTen. These results indicate that fine-grained and integer-exact hybridization outperforms single-mode designs on energy and latency without sacrificing accuracy.

1 INTRODUCTION

Deep Neural Networks (DNNs) are increasingly deployed on edge platforms to enable real-time perception and control in robotics, autonomous systems, and IoT applications (Huang et al., 2017; Wang & Yeung, 2013; Han et al., 2019; Hauswald et al., 2015a;b; He et al., 2015; Krizhevsky et al., 2017; Tan & Le, 2020; Park et al., 2019; Touveron et al., 2022). Artificial Neural Networks (ANNs) achieve state-of-the-art accuracy and fast inference using multiply–accumulate (MAC) operations; however, these dense operations are power intensive. Edge inference imposes stringent latency and energy constraints (LeCun et al., 2015; Chavlis & Poirazi, 2025). Spiking Neural Networks (SNNs) have emerged as an energy-efficient alternative, since they rely on sparse, event-driven, and accumulate-only computations (Xu et al., 2024). As a result, SNNs offer significantly lower energy consumption (Christensen et al., 2022; Fang et al., 2023; Roy et al., 2019), albeit with longer latency due to their temporal processing characteristics.

Modern DNN inference is primarily dominated by matrix multiplications in both fully connected and convolutional layers (Akhlaghi et al., 2018; Albericio et al., 2017; 2016; Ankit et al., 2019; Bankman et al., 2018; Chen et al., 2016; 2019; 2014; Chi et al., 2016a;b; Delmas Lascorz et al., 2019; Ding et al., 2017; Eckert et al., 2018; Esmailzadeh et al., 2012; Gao et al., 2017a;b; 2019; Ghodrati et al., 2020).

These operations are typically expressed using *im2col* (Cho & Brand, 2017; Zhou et al., 2021; Trusov et al., 2021) and are mapped to large General Matrix Multiplication (GEMM) kernels. Empirical analysis shows that a substantial fraction of weights and intermediate activations are zero. Sparsity arises from multiple widely adopted practices: (1) *activation sparsity* in ANNs due to ReLU suppressing negative values, and in SNNs due to threshold-based Leaky Integrate-and-Fire (LIF) spiking dynamics; and (2) *weight sparsity* introduced by pruning and integer quantization. These properties are especially beneficial for edge computing, where 8-bit integer quantization (INT8) is pervasive in deployment frameworks (Wu et al., 2020) and supported by commercial hardware accelerators. Joint exploitation of weight and activation sparsity—*dual sparsity*—can drastically reduce compute and memory traffic (Han et al., 2016a).

Hybrid ANN–SNN models have emerged as a promising solution to achieve an optimal trade-off between inference latency and energy efficiency. Conversion frameworks like PASCAL (Ramesh & Srinivasan, 2025) enable lossless ANN-to-SNN mapping under integer arithmetic, thereby enabling a hybrid ANN-SNN architecture to optimize for energy and latency without compromising accuracy. However, existing hybrid architectures operate at *layer granularity*, activating only one compute style at a time. As a result, significant portions of ANN- or SNN-specific hardware remain idle during inference, leading to suboptimal hardware utilization.

This work introduces **NeuroFlex**, a flexible ANN–SNN accelerator for sparse edge inference. NeuroFlex enables *column-level hybridization*, where each output column in a

¹Indian Institute of Technology Madras, Chennai, Tamil Nadu, India. Correspondence to: Varun Manjunath <ee20b149@smail.iitm.ac.in>.

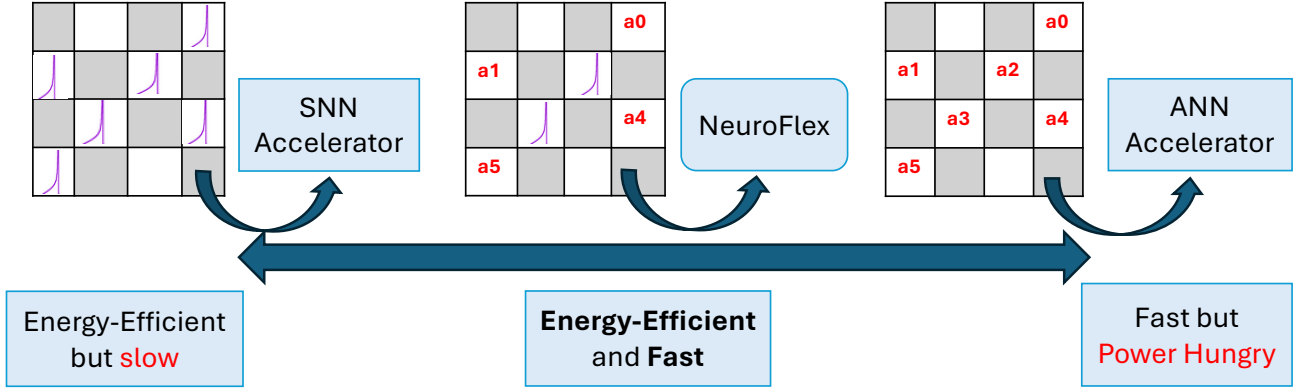


Figure 1. Comparison of execution granularity across accelerators. (Left) SNN-only accelerator: all columns executed as SNNs are energy-efficient but slow. (Right) ANN-only accelerator: all columns executed as ANNs are fast but power hungry. (Center) NeuroFlex enables column-wise hybridization: each output column runs as ANN or SNN based on its cost, achieving high utilization and balancing energy and latency. Empty cells represent zeros.

layer can execute as ANN or SNN while preserving lossless functional equivalence, as shown in Fig. 1. This fine-grained mapping sustains concurrent execution of both domains and maximizes hardware utilization. The scheduler uses offline profiling to optimize the energy-delay cost to determine the execution mode (ANN / SNN) per column before deployment, thus improving runtime efficiency and ensuring deterministic runtime behaviour.

NeuroFlex further exploits dual sparsity using bitmap encoding, a unified compressed FiberCache, and tightly pipelined execution cores. The proposed architecture achieves up to $2.5\times$ speedup over LoAS (Yin et al., 2024) (SNN-only) and $2.51\times$ energy reduction over SparTen (Gondimalla et al., 2019a) (ANN-only), while maintaining baseline accuracy across models. Overall, our key contributions are:

- We extend lossless integer ANN–SNN conversion to *independent column execution*, enabling concurrent hybrid operation within each DNN layer.
- We design NeuroFlex, a unified architecture with shared memory and sparsity-aware compute that sustains one matched non-zero per cycle in both domains.
- We propose an offline energy–delay scheduling mechanism that statically assigns columns to ANN or SNN cores using validation-set workload statistics, avoiding runtime overhead.

The remainder of this paper is organized as follows. Section 2 reviews ANN-SNN conversion, sparsity exploitation algorithms and hardware architectures. Section 3 establishes column-level lossless hybrid ANN-SNN execution. Section 4 details the proposed NeuroFlex architecture. Section 5 presents the cost-based scheduler. Section 7 evaluates

performance against ANN- and SNN-only baselines, while Section 8 concludes our work.

2 RELATED WORK

2.1 ANN-SNN Conversion

Early conversion methods map ReLU activations to firing rates of Integrate and Fire (IF) neurons in order to calibrate thresholds or weights to limit conversion error. This enables deep SNNs on CIFAR/ImageNet, while typically requiring long timesteps and floating-point calibration (Sengupta et al., 2019). More recent work derives conversion error terms and replaces ReLU with Quantization–Clip–Floor–Shift (QCFS) to reduce latency while preserving accuracy using fewer timesteps (Bu et al., 2023). However, these conversion methods still suffer from conversion inaccuracies, especially for larger datasets. PASCAL instead proves a mathematically exact equivalence between an ANN with QCFS activation and its converted SNN with spike inhibition and accumulation per-neuron, yielding lossless integer execution (Ramesh & Srinivasan, 2025).

2.2 Sparse Neural Accelerators

General sparse DNN accelerators compress weights and/or activations to skip ineffectual MACs. EIE pioneered the on-chip execution of pruned and quantized networks with fully-connected layers (Han et al., 2016b). SCNN co-exploits weight and activation sparsity for convolutions with a compressed dataflow using accumulator arrays (Parashar et al., 2017). SparTen introduced native two-sided sparse execution and inner-join support along with software–hardware load balancing (Gondimalla et al., 2019b). GoSPA further optimizes the intersection and reordering for sparse convo-

lutions (Deng et al., 2021).

For SNNs, dual sparsity arises from both the binary spikes and pruned weights. Yin et al. observed that existing SNN accelerators often ignore weight sparsity or suffer timestep-induced dataflow overhead. In order to address that, they proposed a fully temporal-parallel (FTP) dataflow with spike compression and a low-cost inner-join, accelerating sparse-matrix-sparse-matrix kernels central to dual-sparse SNNs. These designs highlight that supporting unstructured weights in conjunction with spike sparsity is necessary to sustain utilization in practice.

2.3 Hybrid ANN-SNN Algorithms and Hardware

Hybrid algorithms combine ANNs and SNNs, thereby achieving a trade-off between accuracy, latency, and power. Aydin et al. presented a “slow-fast” hybrid algorithm, where the SNN states are initialized with an auxiliary ANN operating at a lower rate, to mitigate longer SNN state transients and decay. This helps reduce power with minimal performance losses for event-based pose estimation. Layer-wise hybrid algorithms contain ANN and SNN blocks within a single model to interleave dense and spiking computation. For example, recent surrogate-gradient formulations enable differentiable encode-decode SNN blocks embedded in ANN pipelines (Luu et al., 2025).

Building on algorithmic advances, NEBULA demonstrated a spintronic architecture that supports SNNs, ANNs, and hybrids on a single substrate (Singh et al., 2020). EPHA provides a parallel hybrid accelerator with configurable ANN/SNN modes and reports energy-latency tradeoffs when partitioning models between modes (Zhao et al., 2024). Systems that switch modalities at layer granularity tend to reduce PE utilization during mode transitions or in layers ill-matched to the active mode, motivating co-designs that keep utilization high.

2.4 NeuroFlex: Discussion and Positioning

Previous ANN-SNN conversion methods deliver accuracy with few timesteps but are generally lossy under integer constraints. PASCAL uniquely guarantees integer-preserving equivalence between SNN and QCFS-ANN. Sparse accelerators efficiently exploit activation/weight sparsity but often specialize to either convolutions or dense fully-connected layers, or fail to account for SNN timestep loops. Hybrid ANN-SNN models and chips commonly operate layer-wise across modes, which hurts PE utilization. Our work targets integer-exact conversion while sustaining high utilization under dual sparsity without layer-wise modality switches, addressing these combined gaps.

3 LOSSLESS ANN-SNN CONVERSION AND DATAFLOW

We build on the PASCAL framework (Ramesh & Srinivasan, 2025), which demonstrates a mathematically exact mapping between an ANN with Quantization-Clip-Floor-Shift (QCFS) activation and its converted SNN counterpart. PASCAL achieves this by augmenting the integrate-and-fire (IF) neuron with spike accumulation and inhibition such that the integrate-fire process exactly reproduces the ANN activation statistics. The mathematical equivalence is layerwise and holds under integer arithmetic without approximation.

3.1 Column-Level Extension of PASCAL Equivalence

NeuroFlex extends the PASCAL formulation from layer-level to *column-level* hybrid execution. Each column c in layer l can execute as an ANN or an SNN while maintaining functional equivalence to its reference ANN computation. Since the PASCAL proof of correctness depends only on local integer arithmetic and quantization parameters, the same reasoning applies to each column independently.

Theorem 1 *For any column c operating with integer threshold θ_n and quantization step L_n , the SNN realization \mathcal{M}_c is mathematically equivalent to its ANN realization \mathcal{N}_c , i.e.*

$$f_{\mathcal{M}_c}^z = f_{\mathcal{N}_c}^z, \forall z.$$

Sketch of proof. The result follows from Theorems 3.3–3.6 in (Ramesh & Srinivasan, 2025). The integrate-fire accumulation, thresholding, and reset operations are separable between columns when the arithmetic domain is integer-based. Membrane potential updates depend only on local inputs and thresholds and are independent of neighboring columns. Consequently, the cumulative sum over timesteps in each column converges to the corresponding ANN activation value, thereby maintaining column-wise mathematical equivalence. Further details are in the Appendix.

3.2 Quantization and INT8 Representation

All tensors in NeuroFlex are stored and computed in 8-bit integer (INT8) format. For an 8-level quantization ($L = 8$), lossless conversion between an integer-valued ANN activation and its SNN spike representation requires $(3L - 1) = 23$ timesteps (Ramesh & Srinivasan, 2025). Each timestep encodes a discrete quantization level using binary spikes that preserve the same dynamic range. Because the SNN and ANN representations are equivalent under integer quantization, NeuroFlex stores all intermediate results in ANN (INT8) format. The spike representation is generated *on-the-fly* within the processing element (PE) only when the column executes in SNN mode.

3.3 Hybrid On-the-Fly Dataflow

NeuroFlex maintains all intermediate activations in a unified INT8 format. The scheduler chooses whether each output column is executed as ANN or SNN, and the dataflow adapts accordingly. The conversion between integer ANN activations and temporal SNN spikes is enabled by the PASCAL framework, which provides a lossless equivalence between the two domains. PASCAL achieves functional equivalence between QCFS-ANN and SNN models using three operations:

- **Spike Generation:** converts INT8 ($L=8$) activation value into a deterministic spike train with $(3L - 1)$ timesteps, preserving the same quantized magnitude.
- **Spike Count:** integrates incoming spikes into membrane potential using accumulate-only logic, representing the QCFS quantized activation update over time.
- **Membrane Potential Reinitialization:** applies threshold-based subtraction and state update to maintain exact equivalence to QCFS nonlinear clipping and flooring in the ANN domain.

SNN mode (on-the-fly conversion). The INT8 vector first undergoes **Spike Generation** to form its equivalent temporal spike representation. The spikes are then processed through **Spike Count** and **Membrane Potential Reinitialization** to perform accumulation and threshold updates that exactly match ANN-QCFS semantics. After the temporal window completes, the output is written back to memory in INT8 format. In this mode, the effective number of timesteps remains the same as that specified in (Ramesh & Srinivasan, 2025), since all the steps are carried out, albeit in a different order.

ANN mode. The INT8 vector is directly processed by the MAC units followed by QCFS activation. The resulting INT8 tensor is written back to memory with no temporal execution.

Equivalence. Since both execution paths ingest and produce INT8 representations, column-level mode switching introduces no accuracy loss or storage overhead. ANN and SNN execution behave as interchangeable realizations of the same integer-valued network.

3.4 Dataflow

NeuroFlex employs an inner-product dataflow for both computation modes, as shown in Algorithm 1. In SNN mode, spike accumulation replaces the MAC operation while preserving the operand reuse pattern of inner-product scheduling. This design minimizes partial-sum communication between tiles and maximizes data locality within the PE

cluster. As a result, both ANN and SNN computations share the same data-movement infrastructure, ensuring balanced utilization and consistent latency in mixed-mode execution scenarios.

Algorithm 1 Inner-Product Dataflow with Column-Wise ANN/SNN Execution

```

1: Require: Input activations  $A \in \mathbb{Z}^{M \times K}$  with bitmap  $U \in \{0, 1\}^{M \times K}$ ,
2:   weights  $B \in \mathbb{Z}^{K \times N}$  with bitmap  $X \in \{0, 1\}^{K \times N}$ ,
3:   mode mask  $\text{mode} \in \{\text{ANN}, \text{SNN}\}^N$  (per column),
4:   quantization step  $L$ , spike window (timesteps)  $T = L$ 
5: Ensure: Output activations  $C \in \mathbb{Z}^{M \times N}$ 
6:  $C \leftarrow 0$ 
7: for  $m = 1$  to  $M$  do
8:                                     // row (output) index
9:   for  $n = 1$  to  $N$  do
10:                                     // column index; scheduled as ANN or SNN
11:   if  $\text{mode}[n] == \text{ANN}$  then
12:     for  $k = 1$  to  $K$  do
13:       // inner-product MAC with dual sparsity
14:       if  $U[m, k] = 1$  and  $X[k, n] = 1$  then
15:          $C[m, n] \leftarrow C[m, n] + A[m, k] \cdot B[k, n]$ 
16:       end if
17:     end for
18:      $C[m, n] \leftarrow \text{QCFS}(C[m, n])$ 
19:   else
20:                                     // SNN path (lossless via PASCAL)
21:      $O[1:T] \leftarrow 0$  // timestep buffer (conceptual)
22:     for  $k = 1$  to  $K$  do
23:       // selective spike regeneration after match
24:       if  $U[m, k] = 1$  and  $X[k, n] = 1$  then
25:         // only matched positions
26:          $s \leftarrow \text{SpikeGen}(A[m, k], L)$  //  $s \in \{0, 1\}^T$ 
27:         for  $t = 1$  to  $T$  do
28:           // spatial unrolling over  $t$ 
29:            $O[t] \leftarrow O[t] + s[t] \cdot B[k, n]$  // accumulate
30:         end for
31:       end if
32:     end for
33:     for  $t = 1$  to  $T$  do
34:                                     //  $L-1$  Timesteps
35:        $C[m, n] \leftarrow \text{SpikeCount}(C[m, n], O[t])$ 
36:     end for
37:                                     //  $L$  Timesteps
38:      $C[m, n] \leftarrow \text{SoftResetUpdate}(C[m, n])$ 
39:   end if
40: end for
41: end for

```

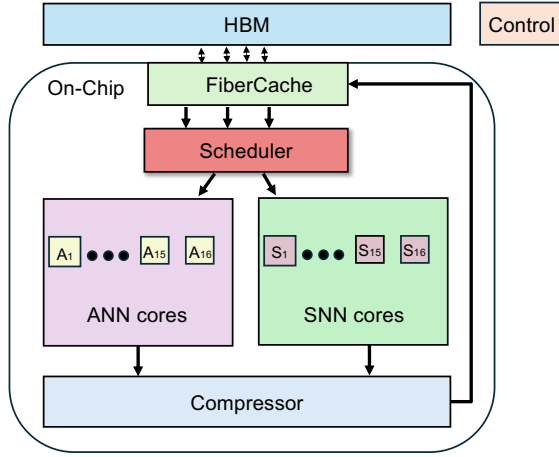


Figure 2. Top-level organization of the proposed NeuroFlex accelerator showing unified memory, shared compressor, FiberCache, and the dual ANN/SNN compute cores.

4 NEUROFLEX ARCHITECTURE

4.1 System Overview

NeuroFlex integrates a pair of heterogeneous computational cores—one optimized for ANN execution and another for SNN execution—within a shared memory hierarchy and interconnect, as shown in Fig. 2. Each core is composed of an array of identical processing elements (PEs). A centralized scheduler dynamically partitions vectors between the two domains, while a shared compressor and unified *FiberCache* exploit data reuse across both workloads. The system follows a feed-through-product (FTP) dataflow that is consistent with the inner-product mapping commonly used in dense ANN accelerators, ensuring spatial and temporal reuse of activations and weights across both computation modes.

4.2 Core Organization

Each core contains multiple PEs that operate on independent vectors streamed from the shared *FiberCache*. The ANN core performs MAC operations followed by QCFS activation. The SNN core executes the PASCAL equivalent integrate-fire sequence using accumulate-only arithmetic. Workloads are dispatched to the cores according to the cost model in Section 5. Within a core, idle PEs are filled greedily to maintain load balance.

4.3 Processing-Element Microarchitecture

Dataflow. Each PE receives a chunk consisting of a bitmap and its corresponding packed non-zero values from the *FiberCache*. The PE processes one non-zero element per cycle, inserting a single bubble between consecutive chunks to synchronize cache fetches. Both cores maintain identi-

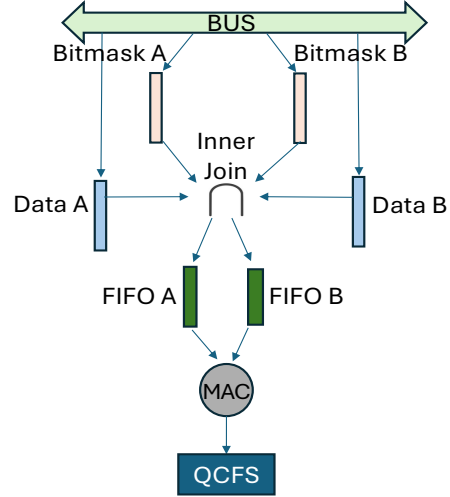


Figure 3. Organization of the ANN core. Each PE performs fetch, prefix alignment, MAC accumulation, and QCFS activation before immediate write-back.

cal control sequencing so that workloads can be reassigned transparently between modes.

ANN PE follows an inner-product dataflow derived from SparTen (Gondimalla et al., 2019a), as shown in Fig. 3. Upon chunk arrival, a fast prefix circuit (Lin & Su, 2005) determines read offsets from the bitmap, and an address generator aligns the corresponding activation and weight streams. The MAC array then accumulates partial sums into a local register tree that overlaps computation across consecutive elements. Once the accumulation for one neuron completes, the QCFS activation stage applies the quantization-clipped nonlinear transform in a single pipeline stage, and the result is written directly to the on-chip SRAM. The pipeline remains fully utilized after an initial two-cycle warm-up.

SNN PE (refer Fig. 4) implements a modified PASCAL dataflow. Two prefix-sum circuits operate sequentially to identify active computation regions. A fast prefix produces early offsets for address alignment, while a laggy prefix completes the accumulation of valid matches between activation (Data A) and weight (Data B) bitmaps. Only activations that correspond to these matched positions are passed on to the spike-generation unit, which converts them into spike packets. This selective regeneration significantly reduces latency and energy overhead, as unnecessary spike encoding for zero or unmatched elements is avoided. The generated spikes enter a pseudo-accumulator that integrates events using quantized integer arithmetic consistent with PASCAL semantics. Correction accumulators apply laggy-prefix (Yin et al., 2024) adjustments in the background, and a soft-reset stage enforces membrane thresholding. The outputs are then re-quantized and written back to SRAM through the shared compressor. The pipeline sustains one matched nonzero

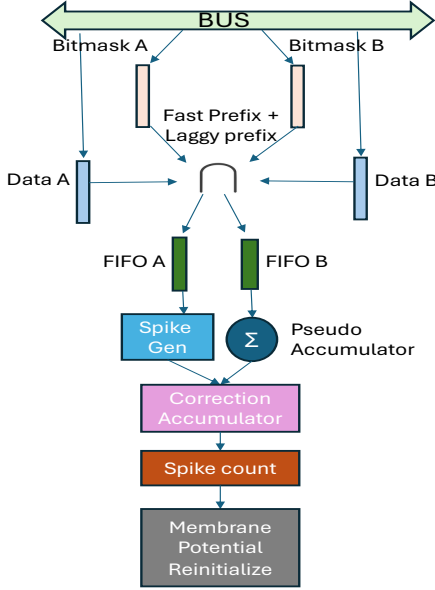


Figure 4. Organization of the SNN core. Each PE includes dual prefix-sum circuits, pseudo-accumulators, and correction accumulators to realize PASCAL-equivalent integrate-and-fire computation. Data A and B correspond to activation inputs and weights, respectively. Only nonzero activations in Data A that match active weights undergo spike generation.

per cycle in steady state while preserving exact equivalence with the ANN computation.

4.4 Compression and FiberCache

NeuroFlex employs a shared compressor located beneath both cores. All data produced by the cores is encoded in bitmap form prior to being written to the on-chip SRAM. Bitmap encoding offers the smallest overhead for integer data, since each element requires only one bit of metadata compared to multi-byte coordinate storage in CSR/CSC formats. The unified FiberCache captures the reuse of both activation and weight fibers. Each cache line contains two parts: (i) a bitmask for the fiber and (ii) a pointer to the continuation line if the fiber extends beyond the capacity of the first line. This design allows concurrent access by multiple PEs through heavy banking, enabling overlapping reads of matrix A and broadcast of compressed matrix B. The cache replacement policy follows the reuse-based schemes described by Li et al.; Zhang et al., which prioritize retaining high-reuse fibers while evicting transient ones, improving cache residency for sparse workloads.

4.5 Data Movement and Interconnect

The shared interconnect is implemented as a swizzle-switch crossbar (Sewell et al., 2012) connecting the FiberCache banks to PE clusters. The crossbar delivers 128-bit chunks

of bitmap and packed values per transfer and maintains one credit of backpressure per chunk to avoid partial-chunk stalls. This design allows sustained one non-zero per-cycle issue across both cores and hides the fetch latency of one cycle per chunk by overlapping computation with data delivery. The FTP dataflow ensures that partial sums are accumulated locally within each PE, minimizing inter-core traffic and memory write-backs.

4.6 Integration with the Scheduler

The scheduler interfaces with both cores through a unified command queue. For each vector, it issues a mode token (ANN or SNN) and assigns it to an available PE. Scheduler decisions are generated offline using the cost function described in Section 5. During runtime, the scheduler performs only lightweight dispatching and load balancing, enabling the architecture to maintain full utilization even under mixed workloads.

5 COST FUNCTION AND SCHEDULING

Hybrid column-level mapping is a discrete assignment problem: every output column of a layer must execute on either the SNN core or the ANN core. Online search is infeasible because the space is exponential in the number of columns and any runtime exploration would add control latency on the critical path. We therefore compute a *static*, validation-driven schedule offline and deploy it as a per-layer bitmask. This section defines the cost model, the surrogate objective we optimize, and the scheduling algorithm. We also provide diagnostic plots illustrating that the surrogate yields near-optimal Energy–Delay Product (EDP) without online tuning, due to higher PE utilization across the cores.

Workload statistics. For each column i and validation sample s , let $r_i^{(s)}$ denote the number of effective multiply matches in its dot product. We summarize runtime variability with a robust statistic per column,

$$\hat{r}_i = \text{Quantile}_q(\{r_i^{(s)}\}_s) \quad (\text{default } q=0.9).$$

The vector $\hat{\mathbf{r}}$ is computed once offline and reused.

Per-core cost model. For core $a \in \{S, A\}$ (SNN, ANN), assigning column i has energy $e_a(i)$ and latency $\ell_a(i)$:

$$e_a(i) = \epsilon_a \hat{r}_i + \zeta_a, \quad \ell_a(i) = \beta_a \hat{r}_i + \delta_a.$$

Coefficients (ϵ_a, β_a) denote the energy consumed per match and the time taken per match respectively. Coefficients (ζ_a, δ_a) capture the fixed per-column overheads. Parameters are calibrated once via microbenchmarks.

Layer cost. Let $X \subseteq \{1, \dots, n\}$ denote columns mapped to the SNN core and \bar{X} be the complement of X . Each

core has P_a PEs; $X_{a,p}$ is the subset placed on PE p . We minimize EDP (Brooks et al., 2000; Rabaey et al., 1997) with energy additivity and makespan-limited latency, as detailed below.

$$E(X) = \sum_{i \in X} e_S(i) + \sum_{i \in \bar{X}} e_A(i), \quad (1)$$

$$T_a(X) = \alpha_a + \max_{p \leq P_a} \sum_{i \in X_{a,p}} \ell_a(i), \quad a \in \{S, A\}, \quad (2)$$

$$D(X) = \max\{T_S(X), T_A(X)\}, \quad (3)$$

$$\text{EDP}(X) = E(X) D(X). \quad (4)$$

Surrogate objective. Directly minimizing $E \cdot D$ is a combinatorial problem. Instead, we use the convex surrogate

$$\Phi(X) = E(X) + \lambda D(X), \quad \lambda > 0,$$

which preserves the energy–latency trade-off and is accurate near the EDP knee. We pick λ such that a 1% decrease in D is worth roughly 0.5–1% increase in E ; the results are insensitive to small changes in λ (Miettinen, 1999; Boyd & Vandenberghe, 2004; Fisher, 1981).

Scheduler. We employ a two-stage *score-then-refine* algorithm, as described in Algorithm 2.

Algorithm 2 Two-Stage Column Assignment and Refinement

- 1: **Stage 1: Per-column scoring and split.**
 - 2: Define a marginal score for assigning column i to core a :

$$S_a(i) = e_a(i) + \lambda \ell_a(i) = (\epsilon_a + \lambda \beta_a) \hat{r}_i + (\zeta_a + \lambda \delta_a).$$
 - 3: Place i on the core with the smaller marginal score.
 - 4: Pack columns within each core using LPT (longest processing time first) with $\ell_a(\cdot)$ as processing times.
 - 5: **Stage 2: Local refinement.**
 - 6: **for** each column **do**
 - 7: Evaluate $\Delta\Phi$ from flipping its core and re-packing only the two affected PEs per core.
 - 8: Commit the best improving move per pass.
 - 9: **end for**
 - 10: Stop on no-improvement or a small pass budget.
-

The complexity of the above algorithm is $O(n \log n)$ (split + LPT) plus $O(n)$ per pass (Graham, 1969; Pinedo, 2008; Garey & Johnson, 1990).

Deployment. For layer ℓ with n_ℓ columns, the compiler emits a bitmask $b_\ell \in \{0, 1\}^{n_\ell}$ and packing seeds; $b_\ell[i]=1$ routes column i to the SNN core. The runtime overhead is

Table 1. NeuroFlex configuration.

Component	Setting
SNN cores	16 PEs, 8-bit weight
ANN cores	16 PEs, 8-bit weight
Inner-join unit	32 inner-join units
Global cache	512 KB, 32 banks, 32-way associative
Crossbars	32×32 and 32×32 , swizzle-switch based
Main memory	128 GB/s over 32×64 -bit HBM channels

minimized because both profiling and search are completed before the inference pass. This also ensures deterministic latency.

The need for offline scheduling. A layer with n columns has 2^n assignments. Even linear-time evaluation per assignment is intractable. Online re-packing also risks instability because the global latency is the max of two core makespans. As a result, small load fluctuations can reshuffle the bottleneck. Offline scheduling over validation statistics provides stable latency and eliminates control overhead.

Cost-space diagnostics. Figure 5A ranks the *marginal efficiency* (energy saved / delay penalty) of moving a single column to the SNN path. The ordering aligns with $S_A(i) - S_S(i)$ from Stage 1, with a handful of inversions fixed by Stage 2 swaps. These diagnostics validate the effectiveness of the simple score and a tiny local search to determine the optimal column mapping. Fig. 5B shows the energy–delay scatter for all assignments of a representative layer, with iso-EDP contours. Points trace a smooth Pareto front; the minimum-EDP solution is near the knee. Our surrogate Φ selects the same solution.

Practical defaults. $q=0.9$ for \hat{r}_i ; three refinement passes; and λ is chosen by a short sweep on a single held-out layer. The resulting per-column bitmasks are fixed and reused across inputs during inference.

6 EXPERIMENTAL METHODOLOGY

6.1 System Configuration

We evaluate NeuroFlex using the configuration in Table 1. The SNN cores perform spike-based computations over 23 timesteps, which is sufficient to achieve lossless conversion, as discussed in Section 3.2.

SNN core microarchitecture. Each SNN PE implements 8 accumulators (one 12-bit pseudo-accumulator and seven 10-bit correction accumulators), one inner-join unit, two depth-8 FIFOs for correction, two 128-bit bitmask buffers, and one 128-byte buffer to hold nonzero weights from Fiber-

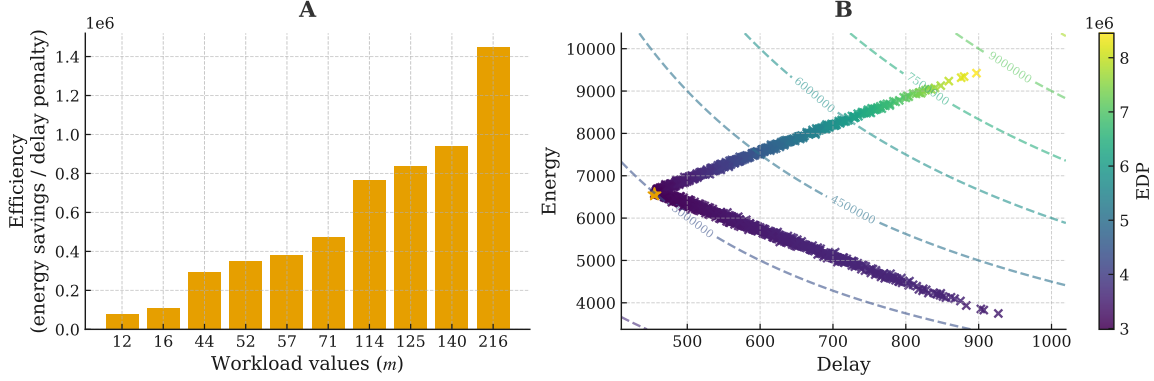


Figure 5. Cost-space diagnostics used in offline scheduling. **A**: marginal efficiency of moving a single column to SNN (energy saved / delay penalty). **B**: energy–delay scatter with iso-EDP contours; the labeled point is the minimum-EDP assignment; m values are the number of matches per column. m used: [12, 16, 44, 52, 57, 71, 114, 125, 140, 216].

Cache. Each inner-join unit integrates one fast prefix-sum circuit and one laggy prefix-sum circuit. The fast prefix-sum produces offsets in a single cycle. The laggy prefix-sum uses 16 adders and a 128-bit buffer to generate offsets in 8 cycles. A spike generator is placed after the inner join. After accumulation, each PE performs the spike-count and spike-update functions.

ANN core microarchitecture. Each ANN PE includes two fast prefix-sum circuits with a FIFO depth 128. After the MAC stage, QCFS activation function is applied. ANN cores share the same 512 KB double-buffered global cache as the SNN cores.

On-chip memory. We allocate 512 KB for the global cache and operate it in a double-buffered mode. Our analysis indicates that this capacity sustains on-chip reuse and keeps PEs busy for the evaluated workloads.

6.2 Baselines and Fairness

We build three baselines, two SNN accelerators (LoAS Yin et al. and Prosperity Wei et al.) and one ANN accelerator (SparTen Gondimalla et al.). We replace the activations in LoAS and Prosperity with PASCAL’s spiking activation, and SparTen’s activation with QCFS. To ensure a fair comparison, all baselines and NeuroFlex use the same total number of PEs and the same global SRAM size. We configure each design with 32 PEs in total and attach the same 512 KB double-buffered global cache. A 128 GB/s HBM subsystem (32×64 -bit channels) serves as off-chip memory for all designs.

6.3 Implementation and Modeling

We implement key components of NeuroFlex and all baselines in RTL and synthesize with Synopsys Design Compiler

at 560 MHz in 40 nm technology node. We use CACTI 7.0 to model the memory structures. We develop a Python cycle-level simulator that tiles loops and maps them to hardware to model execution on NeuroFlex and baselines under identical kernels, dataflows, and memory hierarchies.

7 EXPERIMENTAL RESULTS

We report speedup (higher is better), energy efficiency (higher is better), and Energy–Delay Product (EDP, lower is better). Speedup is normalized to the SNN-only latency. Energy efficiency is normalized to the ANN-only energy. EDP is normalized to SparTen unless noted.

NeuroFlex with the cost-based offline scheduler improves throughput over random mapping by 17.8% for VGG-16, 18.9% for ResNet-34, 16.2% for GoogleNet, and 16.7% for BERT, as shown in Fig. 6. Energy-efficiency also improves for three of the four evaluated models. The gains come from per-column placement by marginal energy-delay trade-off and reduced inter-core makespan (or workload) imbalance. SparTen remains the fastest single-mode baseline, but NeuroFlex closes the gap while delivering up to energy efficiency than ANN-only execution.

Fig. 7 combines latency and energy to plot the energy-delay product (EDP), where lower value indicates better efficiency. NeuroFlex with cost-based scheduling reduces EDP versus SparTen by 65% for VGG-16, 57.5% for ResNet-34, 67.1% for GoogleNet, and 57.4% for BERT. Random scheduling helps but trails the cost-based policy, providing EDP reductions of 45.4%, 43.4%, 44.4%, and 57.6% for the respective models compared to SparTen. The SNN-only baseline achieves the highest energy efficiency, but its longer delay yields between 57.1–69.5% higher EDP than NeuroFlex.

Against Prosperity, NeuroFlex is $13.7\times$ faster with cost-based scheduling and $12.2\times$ faster with random scheduling

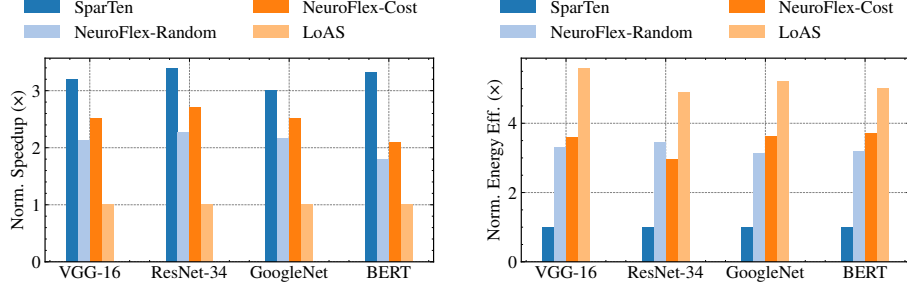


Figure 6. End-to-end speedup and energy-efficiency across models. Bars carry exact values.

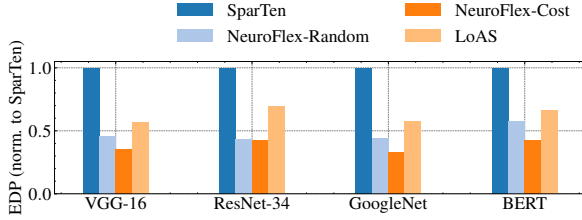


Figure 7. EDP normalized to SparTen (lower is better).

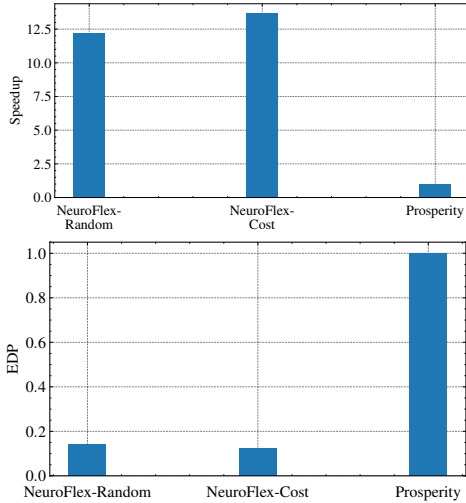


Figure 8. Comparison of NeuroFlex with Prosperity for VGG-16 (Unstructured Sparsity). Top: Speedup comparison; Bottom: EDP comparison.

on VGG-16, as shown in Fig. 8. Although NeuroFlex incurs $1.7\times$ higher energy due to fast prefix operations, the resulting EDP drops to 12.4% (for cost-based scheduling) and 13.9% (for random scheduling) of Prosperity’s, since latency dominates the EDP.

Scalability follows clear patterns. In Fig. 10A, as activation sparsity decreases from 90% to 60% to 25%, relative speed drops from 100% to 21.3% to 12.5% because inner-join opportunities shrink. In Fig. 10B, lower ANN precision and fewer SNN timesteps yield higher throughput: ($L=2, T=5$)

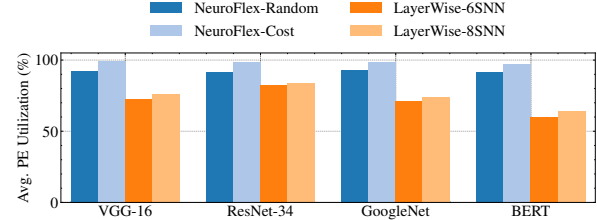


Figure 9. Average PE utilization across models and mapping strategies. *PASCAL-Cost* (our cost-based offline schedule), and *LayerWise- k SNN* (layer-wise hybrid with k SNN layers).

is 100%, (4, 11) is 86%, and (8, 23) is 69%, reflecting heavier compute and longer spike windows. In Fig. 10C, the split of the cores tunes the energy-delay trade-off: Allocating more ANN cores (6/10) raises the speed to 1.12X but reduces the energy efficiency to 86%; Allocating more SNN cores (10/8) raises energy efficiency to 1.15X at 91% speed.

Overall, cost-based offline scheduling is the key lever. It improves throughput by 16–19% versus random mapping, lowers EDP by 57–67% versus SparTen, and preserves deterministic runtime via fixed per-layer bitmasks. NeuroFlex outperforms single-mode accelerators on EDP while enabling explicit speed–energy tuning across sparsity, timesteps/levels, and core provisioning.

PE utilization. Fig. 9 shows that the cost-based scheduling algorithm saturates the array. For VGG-16, ResNet-34, and GoogleNet, *PASCAL-Cost* achieves 99.3%, 98.9%, and 98.6% average PE utilization, respectively, while BERT attains 97.5%. Random column assignment under the same PASCAL framework leaves ~ 7 –8% of throughput on the table, achieving 92.1%, 91.9%, 92.9%, and 91.8% average PE utilization on the respective models. Layer-wise hybridization under-utilizes the fabric due to coarse granularity and inter-layer imbalance, achieving utilization of 71.0–75.9% on VGG-16, 80.9–83.9% on ResNet-34, 70.7–73.7% on GoogleNet, and 60.3–63.9% on BERT. Column-level decisions are therefore the optimal granularity to minimize bubbles on both ANN and SNN cores, and to align work

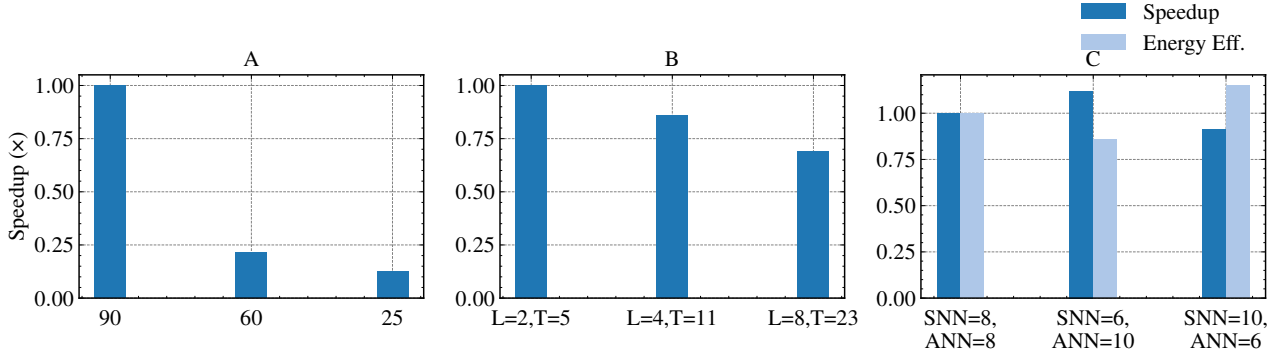


Figure 10. Scalability. **A**: speedup vs activation sparsity. **B**: speedup vs (L, T) (ANN precision, SNN timesteps). **C**: speedup and energy-efficiency vs core split.

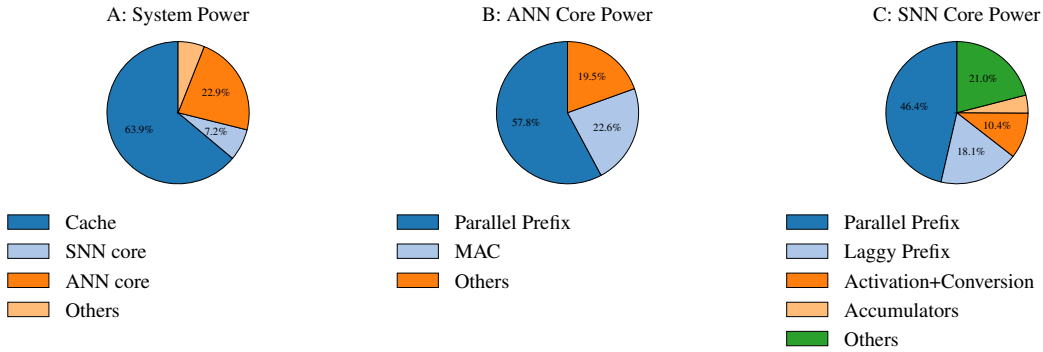


Figure 11. Power analysis. **A**: System-level power breakdown. **B**: ANN core internal breakdown. **C**: SNN core internal breakdown.

with data sparsity and compute intensity at runtime.

Power analysis. Fig. 11A illustrates that the global cache dominates system power (63.9%), followed by the ANN cores (28.88%) and the SNN cores (7.22%). The implication is architectural: improving on-chip data reuse and bank-level concurrency provides larger system gains than micro-optimizing individual computational units in isolation. Within the ANN core (Fig. 11B), parallel-prefix logic (e.g., fast prefix units for dual sparsity) is the primary sink (59%), while MAC units contribute 23.1% and control/others incur 19.9%. Within the SNN core (Fig. 11C), parallel-prefix consumes 44.4%, the laggy prefix contributes 17.3%, activation+conversion 10%, accumulators 3.9%, and others 20.1%. These distributions confirm that dual-sparsity handling is not free, but it remains a minor contributor to system power, as memory traffic dominates.

Activation operators. We also measured the cost of activation units relative to the corresponding datapath primitives. Our ReLU implementation uses $0.8\times$ the power of QCFS, and LIF uses $0.4\times$ the power of the PASCAL algorithm. Both activation engines contribute $< 1\%$ to total system power, so they do not materially shift system budgets while

preserving model accuracy. This, combined with Fig. 11, indicates that system power is governed primarily by memory hierarchy and prefix operations for sparsity processing. Our cost-based mapping reduces the time component (and hence EDP) without increasing the activation overhead.

8 CONCLUSION

In this work, we proposed the NeuroFlex accelerator for fine-grained and integer-exact co-execution of ANNs and SNNs at the column level, which lowers energy-latency cost on sparse edge workloads while preserving accuracy. The design extends QCFS-based ANN-SNN conversion to independent columns, unifies storage with on-the-fly spike generation, and uses an offline cost model to keep ANN and SNN cores busy without runtime overhead. Across standard vision backbones, our scheduler improved throughput and reduced EDP versus strong ANN-only and SNN-only baselines. The key limitation is scope: our approach is valid only for models whose activations can be represented with QCFS. Models that require non-QCFS activations are outside our guarantees. Future work can broaden the activation set, explore workload-aware scheduling, and validate at larger system scales.

REFERENCES

- Akhlaghi, V., Yazdanbakhsh, A., Samadi, K., Gupta, R. K., and Esmaeilzadeh, H. Snapea: Predictive early activation for reducing computation in deep convolutional neural networks. In *2018 ACM/IEEE 45th Annual International Symposium on Computer Architecture (ISCA)*, pp. 662–673, 2018. doi: 10.1109/ISCA.2018.00061.
- Albericio, J., Judd, P., Hetherington, T., Aamodt, T., Jerger, N. E., and Moshovos, A. Cnvlutin: ineffectual-neuron-free deep neural network computing. In *Proceedings of the 43rd International Symposium on Computer Architecture, ISCA '16*, pp. 1–13. IEEE Press, 2016. ISBN 9781467389471. doi: 10.1109/ISCA.2016.11. URL <https://doi.org/10.1109/ISCA.2016.11>.
- Albericio, J., Delm  s, A., Judd, P., Sharify, S., O’Leary, G., Genov, R., and Moshovos, A. Bit-pragmatic deep neural network computing. In *Proceedings of the 50th Annual IEEE/ACM International Symposium on Microarchitecture, MICRO-50 ’17*, pp. 382–394, New York, NY, USA, 2017. Association for Computing Machinery. ISBN 9781450349529. doi: 10.1145/3123939.3123982. URL <https://doi.org/10.1145/3123939.3123982>.
- Ankit, A., Hajj, I. E., Chalamalasetti, S. R., Ndu, G., Foltin, M., Williams, R. S., Faraboschi, P., mei Hwu, W., Strachan, J. P., Roy, K., and Milojicic, D. S. Puma: A programmable ultra-efficient memristor-based accelerator for machine learning inference, 2019. URL <https://arxiv.org/abs/1901.10351>.
- Aydin, A., Gehrig, M., Gehrig, D., and Scaramuzza, D. A hybrid ann–snn architecture for low-power and low-latency visual perception. In *CVPRW*, 2024.
- Bankman, D., Yang, L., Moons, B., Verhelst, M., and Murmann, B. An always-on 3.8µj/86 In *2018 IEEE International Solid-State Circuits Conference - (ISSCC)*, pp. 222–224, 2018. doi: 10.1109/ISSCC.2018.8310264.
- Boyd, S. and Vandenberghe, L. *Convex Optimization*. Cambridge University Press, 2004. Ch. 4, multiobjective scalarization via weighted sums.
- Brooks, D., Tiwari, V., and Martonosi, M. Wattch: A framework for architectural-level power analysis and optimizations. In *ISCA*, 2000.
- Bu, T., Fang, W., Ding, J., Dai, P., Yu, Z., and Huang, T. Optimal ann–snn conversion for high-accuracy and ultra-low-latency spiking neural networks. *arXiv:2303.04347*, 2023.
- Chavlis, S. and Poirazi, P. Dendrites endow artificial neural networks with accurate, robust and parameter-efficient learning. *Nature Communications*, 16(1):943, 2025. doi: 10.1038/s41467-025-56297-9.
- Chen, Y., Luo, T., Liu, S., Zhang, S., He, L., Wang, J., Li, L., Chen, T., Xu, Z., Sun, N., and Temam, O. Dadi-annao: A machine-learning supercomputer. *2014 47th Annual IEEE/ACM International Symposium on Microarchitecture*, pp. 609–622, 2014. URL <https://api.semanticscholar.org/CorpusID:6838992>.
- Chen, Y.-H., Emer, J., and Sze, V. Eyeriss: a spatial architecture for energy-efficient dataflow for convolutional neural networks. In *Proceedings of the 43rd International Symposium on Computer Architecture, ISCA ’16*, pp. 367–379. IEEE Press, 2016. ISBN 9781467389471. doi: 10.1109/ISCA.2016.40. URL <https://doi.org/10.1109/ISCA.2016.40>.
- Chen, Y.-H., Yang, T.-J., Emer, J., and Sze, V. Eyeriss v2: A flexible accelerator for emerging deep neural networks on mobile devices. *IEEE Journal on Emerging and Selected Topics in Circuits and Systems*, 9(2):292–308, 2019. doi: 10.1109/JETCAS.2019.2910232.
- Chi, P., Li, S., Xu, C., Zhang, T., Zhao, J., Liu, Y., Wang, Y., and Xie, Y. Prime: a novel processing-in-memory architecture for neural network computation in reram-based main memory. *SIGARCH Comput. Archit. News*, 44(3):27–39, June 2016a. ISSN 0163-5964. doi: 10.1145/3007787.3001140. URL <https://doi.org/10.1145/3007787.3001140>.
- Chi, P., Li, S., Xu, C., Zhang, T., Zhao, J., Liu, Y., Wang, Y., and Xie, Y. Prime: a novel processing-in-memory architecture for neural network computation in reram-based main memory. In *Proceedings of the 43rd International Symposium on Computer Architecture, ISCA ’16*, pp. 27–39. IEEE Press, 2016b. ISBN 9781467389471. doi: 10.1109/ISCA.2016.13. URL <https://doi.org/10.1109/ISCA.2016.13>.
- Cho, M. and Brand, D. Mec: Memory-efficient convolution for deep neural network, 2017. URL <https://arxiv.org/abs/1706.06873>.
- Christensen, D. V., Dittmann, R., Linares-Barranco, B., Sebastian, A., Le Gallo, M., Redaelli, A., Slesazeck, S., Mikolajick, T., Spiga, S., Menzel, S., Valov, I., Milano, G., Ricciardi, C., Liang, S.-J., Miao, F., Lanza, M., Quill, T. J., Keene, S. T., Salleo, A., Grollier, J., Markovi  , D., Mizrahi, A., Yao, P., Yang, J. J., Indiveri, G., Strachan, J. P., Datta, S., Vianello, E., Valentian, A., Feldmann, J., Li, X., Pernice, W. H. P., Bhaskaran, H., Furber, S., Neftci, E., Scherr, F., Maass, W., Ramaswamy, S., Tapson, J., Panda, P., Kim, Y., Tanaka, G., Thorpe, S., Bartolozzi, C., Cleland, T. A., Posch, C., Liu, S.-C., Panuccio, G., Mahmud, M., Mazumder, A. N., Hosseini, M., Mohsenin,

- T., Donati, E., Tolu, S., Galeazzi, R., Christensen, M. E., Holm, S., Ielmini, D., and Pryds, N. 2022 roadmap on neuromorphic computing and engineering. *Neuromorphic Computing and Engineering*, 2(2):022501, 2022. doi: 10.1088/2634-4386/ac4a83.
- Delmas Lascorz, A., Judd, P., Stuart, D. M., Poulos, Z., Mahmoud, M., Sharify, S., Nikolic, M., Siu, K., and Moshovos, A. Bit-tactical: A software/hardware approach to exploiting value and bit sparsity in neural networks. In *Proceedings of the Twenty-Fourth International Conference on Architectural Support for Programming Languages and Operating Systems*, ASPLOS '19, pp. 749–763, New York, NY, USA, 2019. Association for Computing Machinery. ISBN 9781450362405. doi: 10.1145/3297858.3304041. URL <https://doi.org/10.1145/3297858.3304041>.
- Deng, C. et al. Gspa: An energy-efficient high-performance globally optimized sparse cnn accelerator. In *ISCA*, 2021.
- Ding, C., Liao, S., Wang, Y., Li, Z., Liu, N., Zhuo, Y., Wang, C., Qian, X., Bai, Y., Yuan, G., Ma, X., Zhang, Y., Tang, J., Qiu, Q., Lin, X., and Yuan, B. C_{ir}/scp_c cnn: accelerating and compressing deep neural networks using block-circulant weight matrices. In *Proceedings of the 50th Annual IEEE/ACM International Symposium on Microarchitecture*, MICRO-50, pp. 395–408. ACM, October 2017. doi: 10.1145/3123939.3124552. URL <http://dx.doi.org/10.1145/3123939.3124552>.
- Eckert, C., Wang, X., Wang, J., Subramanian, A., Iyer, R., Sylvester, D., Blaauw, D., and Das, R. Neural cache: Bit-serial in-cache acceleration of deep neural networks, 2018. URL <https://arxiv.org/abs/1805.03718>.
- Esmailzadeh, H., Sampson, A., Ceze, L., and Burger, D. Neural acceleration for general-purpose approximate programs. In *2012 45th Annual IEEE/ACM International Symposium on Microarchitecture*, pp. 449–460, 2012. doi: 10.1109/MICRO.2012.48.
- Fang, W., Chen, Y., Ding, J., Yu, Z., Masquelier, T., Chen, D., Huang, L., Zhou, H., Li, G., and Tian, Y. Spikingjelly: An open-source machine learning infrastructure platform for spike-based intelligence. *Science Advances*, 9(40): eadi1480, 2023. doi: 10.1126/sciadv.adi1480.
- Fisher, M. L. The lagrangian relaxation method for integer programming. *Management Science*, 27(1):1–18, 1981.
- Gao, M., Pu, J., Yang, X., Horowitz, M., and Kozyrakis, C. Tetris: Scalable and efficient neural network acceleration with 3d memory. *SIGARCH Comput. Archit. News*, 45(1):751–764, April 2017a. ISSN 0163-5964. doi: 10.1145/3093337.3037702. URL <https://doi.org/10.1145/3093337.3037702>.
- Gao, M., Pu, J., Yang, X., Horowitz, M., and Kozyrakis, C. Tetris: Scalable and efficient neural network acceleration with 3d memory. In *Proceedings of the Twenty-Second International Conference on Architectural Support for Programming Languages and Operating Systems*, ASPLOS '17, pp. 751–764, New York, NY, USA, 2017b. Association for Computing Machinery. ISBN 9781450344654. doi: 10.1145/3037697.3037702. URL <https://doi.org/10.1145/3037697.3037702>.
- Gao, M., Yang, X., Pu, J., Horowitz, M., and Kozyrakis, C. Tangram: Optimized coarse-grained dataflow for scalable nn accelerators. In *Proceedings of the Twenty-Fourth International Conference on Architectural Support for Programming Languages and Operating Systems*, ASPLOS '19, pp. 807–820, New York, NY, USA, 2019. Association for Computing Machinery. ISBN 9781450362405. doi: 10.1145/3297858.3304014. URL <https://doi.org/10.1145/3297858.3304014>.
- Garey, M. R. and Johnson, D. S. *Computers and Intractability: A Guide to the Theory of NP-Completeness*. W. H. Freeman & Co., USA, 1990. ISBN 0716710455.
- Ghodrati, S., Ahn, B. H., Kyung Kim, J., Kinzer, S., Yatham, B. R., Alla, N., Sharma, H., Alian, M., Ebrahimi, E., Kim, N. S., Young, C., and Esmailzadeh, H. Planaria: Dynamic architecture fission for spatial multi-tenant acceleration of deep neural networks. In *2020 53rd Annual IEEE/ACM International Symposium on Microarchitecture (MICRO)*, pp. 681–697, 2020. doi: 10.1109/MICRO50266.2020.00062.
- Gondimalla, A., Chesnut, N., Thottethodi, M., and Vijaykumar, T. N. Sparten: A sparse tensor accelerator for convolutional neural networks. In *Proceedings of the 52nd Annual IEEE/ACM International Symposium on Microarchitecture*, MICRO-52, pp. 151–165, New York, NY, USA, 2019a. Association for Computing Machinery. ISBN 9781450369381. doi: 10.1145/3352460.3358291. URL <https://doi.org/10.1145/3352460.3358291>.
- Gondimalla, A. et al. Sparten: A sparse tensor accelerator for convolutional neural networks. In *ASPLOS*, 2019b.
- Graham, R. L. Bounds on multiprocessing timing anomalies. *SIAM Journal on Applied Mathematics*, 17(2):416–429, 1969. ISSN 00361399. URL <http://www.jstor.org/stable/2099572>.
- Han, K. J., Prieto, R., Wu, K., and Ma, T. State-of-the-art speech recognition using multi-stream self-attention with dilated 1d convolutions, 2019. URL <https://arxiv.org/abs/1910.00716>.

- Han, S., Liu, X., Mao, H., Pu, J., Pedram, A., Horowitz, M. A., and Dally, W. J. Eie: Efficient inference engine on compressed deep neural network, 2016a. URL <https://arxiv.org/abs/1602.01528>.
- Han, S. et al. Eie: Efficient inference engine on compressed deep neural network. In *ISCA*, 2016b.
- Hauswald, J., Laurenzano, M. A., Zhang, Y., Li, C., Rovinski, A., Khurana, A., Dreslinski, R. G., Mudge, T., Petrucci, V., Tang, L., and Mars, J. Sirius: An open end-to-end voice and vision personal assistant and its implications for future warehouse scale computers. In *Proceedings of the Twentieth International Conference on Architectural Support for Programming Languages and Operating Systems*, ASPLOS '15, pp. 223–238, New York, NY, USA, 2015a. Association for Computing Machinery. ISBN 9781450328357. doi: 10.1145/2694344.2694347. URL <https://doi.org/10.1145/2694344.2694347>.
- Hauswald, J., Laurenzano, M. A., Zhang, Y., Li, C., Rovinski, A., Khurana, A., Dreslinski, R. G., Mudge, T., Petrucci, V., Tang, L., and Mars, J. Sirius: An open end-to-end voice and vision personal assistant and its implications for future warehouse scale computers. *SIGPLAN Not.*, 50(4):223–238, March 2015b. ISSN 0362-1340. doi: 10.1145/2775054.2694347. URL <https://doi.org/10.1145/2775054.2694347>.
- He, K., Zhang, X., Ren, S., and Sun, J. Deep residual learning for image recognition, 2015. URL <https://arxiv.org/abs/1512.03385>.
- Huang, G., Liu, Z., Van Der Maaten, L., and Weinberger, K. Q. Densely connected convolutional networks. In *2017 IEEE Conference on Computer Vision and Pattern Recognition (CVPR)*, pp. 2261–2269, 2017. doi: 10.1109/CVPR.2017.243.
- Krizhevsky, A., Sutskever, I., and Hinton, G. E. Imagenet classification with deep convolutional neural networks. *Commun. ACM*, 60(6):84–90, May 2017. ISSN 0001-0782. doi: 10.1145/3065386. URL <https://doi.org/10.1145/3065386>.
- LeCun, Y., Bengio, Y., and Hinton, G. Deep learning. *Nature*, 521(7553):436–444, 2015. doi: 10.1038/nature14539.
- Li, Z., Li, J., Chen, T., Niu, D., Zheng, H., Xie, Y., and Gao, M. Spada: Accelerating sparse matrix multiplication with adaptive dataflow. In *Proceedings of the 28th ACM International Conference on Architectural Support for Programming Languages and Operating Systems, Volume 2*, ASPLOS 2023, pp. 747–761, New York, NY, USA, 2023. Association for Computing Machinery. ISBN 9781450399166. doi: 10.1145/3575693.3575706. URL <https://doi.org/10.1145/3575693.3575706>.
- Lin, Y.-C. and Su, C.-Y. Faster optimal parallel prefix circuits: New algorithmic construction. *Journal of Parallel and Distributed Computing*, 65(12):1585–1595, 2005. ISSN 0743-7315. doi: <https://doi.org/10.1016/j.jpdc.2005.05.017>. URL <https://www.sciencedirect.com/science/article/pii/S0743731505001346>.
- Luu, N. T., Luu, D. T., Nam, P. N., and Thang, T. C. Hybrid layer-wise ann–snn with surrogate spike encoding–decoding structure. *arXiv:2509.24411*, 2025.
- Miettinen, K. *Nonlinear Multiobjective Optimization*. Kluwer, 1999.
- Parashar, A. et al. Scnn: An accelerator for compressed-sparse convolutional neural networks. In *ISCA*, 2017.
- Park, D. S., Chan, W., Zhang, Y., Chiu, C.-C., Zoph, B., Cubuk, E. D., and Le, Q. V. SpecAugment: A simple data augmentation method for automatic speech recognition. In *Interspeech 2019*, interspeech2019. ISCA, September 2019. doi: 10.21437/interspeech.2019-2680. URL <http://dx.doi.org/10.21437/Interspeech.2019-2680>.
- Pinedo, M. L. *Scheduling: Theory, Algorithms, and Systems*. Springer Publishing Company, Incorporated, 3rd edition, 2008. ISBN 0387789340.
- Rabaey, J., Chandrakasan, A., and Nikolic, B. Low-power digital design. *Proceedings of the IEEE*, 1997. Popularizes energy–delay style objectives.
- Ramesh, P. and Srinivasan, G. Pascal: Precise and efficient ann–snn conversion using spike accumulation and adaptive layerwise activation, 2025. URL <https://arxiv.org/abs/2505.01730>.
- Roy, K., Jaiswal, A., and Panda, P. Towards spike-based machine intelligence with neuromorphic computing. *Nature*, 575(7784):607–617, 2019. doi: 10.1038/s41586-019-1677-2.
- Sengupta, A., Ye, Y., Wang, R., Liu, C., and Roy, K. Going deeper in spiking neural networks: Vgg and residual architectures. *arXiv:1802.02627*, 2019.
- Sewell, K., Dreslinski, R. G., Manville, T., Satpathy, S., Pinckney, N., Blake, G., Cieslak, M., Das, R., Wenisch, T. F., Sylvester, D., Blaauw, D., and Mudge, T. Swizzle-switch networks for many-core systems. *IEEE Journal*

- on *Emerging and Selected Topics in Circuits and Systems*, 2(2):278–294, 2012. doi: 10.1109/JETCAS.2012.2193936.
- Singh, S. et al. Nebula: A neuromorphic spin-based ultra-low power architecture for snns and anns. In *ISCA*, 2020.
- Tan, M. and Le, Q. V. Efficientnet: Rethinking model scaling for convolutional neural networks, 2020. URL <https://arxiv.org/abs/1905.11946>.
- Touvron, H., Vedaldi, A., Douze, M., and Jégou, H. Fixing the train-test resolution discrepancy, 2022. URL <https://arxiv.org/abs/1906.06423>.
- Trusov, A. V., Limonova, E. E., Nikolaev, D. P., and Ar-lazarov, V. V. p-im2col: Simple yet efficient convolution algorithm with flexibly controlled memory overhead. *IEEE Access*, 9:168162–168184, 2021. doi: 10.1109/ACCESS.2021.3135690.
- Wang, N. and Yeung, D.-Y. Learning a deep compact image representation for visual tracking. In Burges, C., Bottou, L., Welling, M., Ghahramani, Z., and Weinberger, K. (eds.), *Advances in Neural Information Processing Systems*, volume 26. Curran Associates, Inc., 2013. URL https://proceedings.neurips.cc/paper_files/paper/2013/file/dc6a6489640ca02b0d42dabeb8e46bb7-Paper.pdf.
- Wei, C., Guo, C., Cheng, F., Li, S., Yang, H. F., Li, H. H., and Chen, Y. Prosperity: Accelerating spiking neural networks via product sparsity, 2025. URL <https://arxiv.org/abs/2503.03379>.
- Wu, H., Judd, P., Zhang, X., Isaev, M., and Micikevicius, P. Integer quantization for deep learning inference: Principles and empirical evaluation, 2020. URL <https://arxiv.org/abs/2004.09602>.
- Xu, Y., Tang, G., Yousefzadeh, A., de Croon, G., and Sifalakis, M. Event-based optical flow on neuromorphic processor: Ann vs. snn comparison based on activation sparsification, 2024. URL <https://arxiv.org/abs/2407.20421>.
- Yin, R., Kim, Y., Wu, D., and Panda, P. Loas: Fully temporal-parallel dataflow for dual-sparse spiking neural networks, 2024. URL <https://arxiv.org/abs/2407.14073>.
- Zhang, G., Attaluri, N., Emer, J. S., and Sanchez, D. Gamma: leveraging gustavson’s algorithm to accelerate sparse matrix multiplication. In *Proceedings of the 26th ACM International Conference on Architectural Support for Programming Languages and Operating Systems*, ASPLOS ’21, pp. 687–701, New York, NY, USA, 2021. Association for Computing Machinery. ISBN 9781450383172. doi: 10.1145/3445814.3446702. URL <https://doi.org/10.1145/3445814.3446702>.
- Zhao, Y. et al. Epha: An energy-efficient parallel hybrid architecture for anns and snns. *ACM TODAES*, 2024.
- Zhou, Y., Yang, M., Guo, C., Leng, J., Liang, Y., Chen, Q., Guo, M., and Zhu, Y. Characterizing and demystifying the implicit convolution algorithm on commercial matrix-multiplication accelerators. *CoRR*, abs/2110.03901, 2021. URL <https://arxiv.org/abs/2110.03901>.

9 APPENDIX

9.1 Proof For Column Level Equivalence

We use the definitions of *classification maps* and *mathematical equivalence* from (Ramesh & Srinivasan, 2025), and re-formulate the theorems to ensure that they work for INT8 computation. We state the relevant corollaries below which invoke corresponding theorems in (Ramesh & Srinivasan, 2025).

Corollary 1.1 *A model with quantization step L_n and threshold θ_n such that $\frac{\theta_n}{L_n}$ is an integer and θ_n is within the range of INT8 in the input layer satisfies the input layer equivalence as stated in Theorem 3.5 in (Ramesh & Srinivasan, 2025)*

Corollary 1.2 *A layer with quantization step L , performing a MatMul operation followed by Batch Normalization, i.e. $z^{l+1} = \gamma \cdot \frac{(z^l * W) + b - \mu}{\sqrt{\sigma^2 + \epsilon}} + \beta$ such that each of the quantities $b' = \frac{b}{L}, \mu' = \frac{\mu}{L}, \beta' = \frac{\beta}{L}$ and $\frac{\gamma}{\sqrt{\sigma^2 + \epsilon}}$ are integers within the limits of INT8 satisfies Theorem 3.3 in (Ramesh & Srinivasan, 2025)*

Corollaries 1.1 and 1.2, along with Theorem 3.4 in (Ramesh & Srinivasan, 2025) is sufficient to show that the INT8-PASC formulation is equivalent to the corresponding INT8-source ANN (Theorem 3.6 in (Ramesh & Srinivasan, 2025)).

The proofs of the corollaries are exactly the same as the proofs for the corresponding theorems in (Ramesh & Srinivasan, 2025), with the appropriate assumptions to ensure that the precision of division is maintained in the INT8 computation.